



**HAL**  
open science

## Turbulent flows in straight compound open-channel with a transverse embankment on the floodplain

Y. Peltier, Sébastien Proust, N. Rivière, André Paquier, K. Shiono

### ► To cite this version:

Y. Peltier, Sébastien Proust, N. Rivière, André Paquier, K. Shiono. Turbulent flows in straight compound open-channel with a transverse embankment on the floodplain. *Journal of Hydraulic Research*, 2013, 51 (4), p. 446 - p. 458. 10.1080/00221686.2013.796499 . hal-01073136

**HAL Id: hal-01073136**

**<https://hal.science/hal-01073136>**

Submitted on 9 Oct 2014

**HAL** is a multi-disciplinary open access archive for the deposit and dissemination of scientific research documents, whether they are published or not. The documents may come from teaching and research institutions in France or abroad, or from public or private research centers.

L'archive ouverte pluridisciplinaire **HAL**, est destinée au dépôt et à la diffusion de documents scientifiques de niveau recherche, publiés ou non, émanant des établissements d'enseignement et de recherche français ou étrangers, des laboratoires publics ou privés.

1 Turbulent flows in straight compound open-channel with a transverse  
2 embankment on the floodplain

3 YANN PELTIER (IAHR Member), Ph. D., Laboratoire de Mécanique des Fluides et  
4 Acoustique (LMFA, CNRS UMR5509, Université de Lyon), INSA de Lyon, Bât. Jacquard,  
5 20 av. A. Einstein, 69621, Villeurbanne, France. Previously, Irstea, UR HHLY, Hydrology-  
6 Hydraulics, 5 rue de la Doua, CS 70077, 69626 VILLEURBANNE Cedex, France.

7 *Email: yann.peltier90@gmail.com (Corresponding Author)*

8 SEBASTIEN PROUST (IAHR Member), Researcher, Irstea, UR HHLY, Hydrology-  
9 Hydraulics, 5 rue de la Doua, CS 70077, 69626 VILLEURBANNE Cedex, France.

10 *Email: sebastien.proust@irstea.fr*

11 NICOLAS RIVIERE (IAHR Member), Professor, Laboratoire de Mécanique des Fluides et  
12 Acoustique (LMFA, CNRS UMR5509, Université de Lyon), INSA de Lyon, Bât. Jacquard,  
13 20 av. A. Einstein, 69621, Villeurbanne, France.

14 *Email: nicolas.riviere@insa-lyon.fr*

15 ANDRE PAQUIER (IAHR Member), Senior Researcher, Irstea, UR HHLY, Hydrology-  
16 Hydraulics, 5 rue de la Doua, CS 70077, 69626 VILLEURBANNE Cedex, France.

17 *Email: andre.paquier@irstea.fr*

18 KOJI SHIONO (IAHR Member), Professor, Department of Civil and Building Engineering,  
19 Loughborough University, Leicestershire, UKLE11 3TU, United Kingdom.

20 *Email: k.shiono@lboro.ac.uk*

21

## 22 Turbulent flows in straight compound open-channel with a transverse 23 embankment on the floodplain

### 24 **ABSTRACT**

25 The present study deals with turbulent flows in an asymmetrical compound channel with an  
26 embankment set on the floodplain, perpendicularly to the longitudinal direction. The main purpose of  
27 this study was to assess how a rapidly varied flow affects interaction between the floodplain flow and  
28 the main channel flow. In addition to rapid changes in the water level and velocity across the  
29 compound channel that have a great influence on the boundary shear stress distribution, the  
30 embankment, through two recirculation zones developing upstream and downstream, is also  
31 responsible for strong lateral mass exchange between the main channel and the floodplains (channel  
32 sub-sections). The lateral velocity can indeed reach 50 % of the longitudinal velocity, which modifies  
33 the characteristics of the mixing layer developing between the channel sub-sections. Depth-averaged  
34 Reynolds shear stresses 5 times greater than those measured for reference flows are recorded within the  
35 mixing layer, which indicates that the turbulent exchange is also impacted by the lateral mass  
36 exchange.

37 **Keywords:** Flood modelling, Flow-structure interactions, Laboratory studies, Separated flows,  
38 Turbulent mixing layers.

### 39 **1. Introduction**

40 In natural or engineered rivers, the flow is contained in the main channel (*m*), limited by the  
41 river banks, most of the time. During heavy snow melting events or significant rainfalls, the  
42 river main channel cannot convey all the runoff and consequently overflows on its adjacent  
43 floodplains (*f*). The resulting flow is identified as a compound channel flow.

44 Under uniform flow conditions, the fast and deep flow in the main channel interacts  
45 with the slow and shallow flow on the floodplains. This results in the formation of a mixing  
46 layer at the interface between the sub-sections (the main channel and the floodplains), which  
47 transfers momentum due to turbulent exchange between them (Sellin 1964). This turbulent  
48 exchange leads to the decrease in the main channel conveyance and to the increase on the  
49 floodplain one. Moreover, the overall conveyance of the compound channel is reduced  
50 relative to the one of a single channel of same hydraulic radius (Knight and Demetriou 1983,  
51 Knight and Hamed 1984).

52 Knight and Shiono (1990) and Shiono and Knight (1991) showed that for such flow  
53 conditions, the depth-averaged Reynolds shear stress representative of the turbulent exchange,  
54  $T_{xy} = \langle -\rho \overline{u'v'} \rangle$  ( $u'$  and  $v'$  the horizontal components of the fluctuating velocity,  $\langle \rangle$  the

55 depth-averaging operator and  $\bar{\quad}$  the time-averaging operator), is maximal at the junction  
56 between the sub-sections. They also found that for a given floodplain width, the lateral extent  
57 of the high shear region between the channel sub-sections and the maximum of  $T_{xy}$ , are  
58 inversely proportional to the relative flow depth,  $H_r = H_f/H_m$  ( $H_f$  and  $H_m$ , the mean water depth  
59 on the floodplain and in the main channel respectively), while they increase with the  
60 floodplain width and a constant  $H_r$ . According to van Prooijen *et al.* (2005), the behaviour of  
61  $T_{xy}$  within the mixing layer must be linked to the difference in velocity between the sub-  
62 sections,  $U_m - U_f$  ( $U_m$  and  $U_f$  are the longitudinal mean velocity in the main channel and on  
63 the floodplain respectively), and to the lateral gradient of the depth-averaged longitudinal  
64 velocity,  $\partial U_d / \partial y$ .

65 The turbulent exchange between the sub-sections also depends on channel geometries  
66 according to results of three types of geometries, which were studied in the past:

- 67 • Prismatic geometry with a disequilibrium in the upstream discharge distribution  
68 (Bousmar *et al.* 2005, Proust *et al.* 2011, 2013),
- 69 • Non prismatic geometry with a continuous variation in the floodplain width, the  
70 overall width being constant along the channel, as skewed compound channels (Elliot  
71 and Sellin 1990, Chlebek and Knight 2008) and compound meandering channels  
72 (Shiono and Muto 1998),
- 73 • Non prismatic geometry with a variable overall width, as symmetrically converging  
74 floodplains (Bousmar *et al.* 2004), symmetrically diverging floodplains (divergence  
75 angle smaller than 5.8°; Proust 2005, Bousmar *et al.* 2006) and compound channel  
76 with an abrupt floodplain contraction (convergence angle of 22°; Proust *et al.* 2006).

77 These flows were defined as gradually varied flows. In these experiments, each channel either  
78 yields or receives water from its adjacent channel(s); this exchange of mass, along with non-  
79 negligible lateral velocities, generates noticeable additional lateral exchange of streamwise  
80 momentum that superimposes to the turbulent exchange between the sub-sections (Proust *et*  
81 *al.* 2009, 2010). According to Proust *et al.* (2013), the direction and the intensity of the lateral  
82 velocity induce changes in the lateral distribution of the local Reynolds shear stress,  $-\rho \overline{u'v'}$   
83  $-\rho \overline{u'v'}$ , by stretching the coherent structures that develop inside the mixing layer. When  
84 mass is transferred from the floodplain to the main channel, the region of high turbulent shear  
85 is displaced towards the main channel. Both the maximum of  $T_{xy}$  and the lateral extent of the  
86 high shear region are lowered. When mass is transferred towards the floodplains, the high  
87 shear region widely extends on the floodplains and the peak of  $T_{xy}$  at the sub-sections junction  
88 is enhanced.

89 In natural or manmade rivers, the floodplains may rapidly vary with obstacles either  
90 natural (natural levees, rock slide) or artificial (embankments for railways and motorways).

91 This has various implications for risk assessment and river geomorphology. The considered  
92 embankment here acts as an asymmetric, partial dam which causes an elevation of the water  
93 depth in the whole upstream channel. The flow on the floodplain is then constricted by the  
94 obstacle, which promotes the development of two recirculation zones, one upstream from the  
95 obstacle and one downstream. Silting can occur in these slack-flows. Oppositely, the flow has  
96 to skirt the embankment and its acceleration, causes scouring and can possibly blow away  
97 goods or people. When focusing on the flow description, it results in significant variations of  
98 the flow section and in the generation of strong lateral mass exchange (relatively to gradually  
99 varied flows) between the sub-sections (Proust 2005, Bourdat 2007, Peltier *et al.* 2008, 2009).  
100 This type of flow commonly occurs in the fields, but has been rarely studied. Among the few  
101 studies dealing with overbank flows with an obstacle on the floodplain (Proust 2005, Peltier *et*  
102 *al.* 2008), the results indicated that 2D-H numerical modelling has some difficulties in  
103 capturing the recirculating flows and that the physics of the mixing layers in the channel is  
104 still not well understood. Additional detailed measurements of the turbulence characteristics  
105 and of boundary shear stress are required, along with some theoretical developments. The  
106 understanding of overbank flows in compound channel with a transversal obstacle blocking  
107 off the floodplain is indeed paramount for flood modellers. The accurate estimation of the  
108 characteristics of the one hundred year return period flood, for instance, is necessary for  
109 designing unsinkable motorway and railway embankments (Lefort and Tanguy 2009).  
110 Moreover, as part of the establishment of flood hazard prevention plans, flooded area in the  
111 vicinity of embankments must be determined with minimal uncertainties.

112 The present study then aims at assessing the effects on the hydraulic parameters of the  
113 superposition of two types of flows: (i) a rapidly varied flow in the vicinity of a thin  
114 embankment and (ii) a compound channel flow. We notably estimate the effects of the lateral  
115 mass exchange on the interaction between the flows in the sub-sections.

## 116 **2. Experimental setup**

### 117 *2.1. The compound channel*

118 The present experiments were conducted in an experimental flume located at the Laboratoire  
119 de Mécanique des Fluides et d'Acoustique (LMFA, Lyon, France). The flume has a length,  $L$ ,  
120 of 8 m and a total width,  $B$ , of 1.2 m. This flume is straight with an asymmetrical cross-  
121 section and has a longitudinal bed-slope,  $S_{0x}$ , of 0.18 %. The main channel cross-section is  
122 rectangular (Figure 1) and is 0.4 m wide. The bank-full height,  $b$ , is of 5.1 cm and the  
123 floodplain is 0.8 m wide. The floodplain and the main channel are PVC made and their  
124 surface state is smooth.

125           Following the recommendations of Bousmar *et al.* (2005), separated inlet tanks for  
126 the main channel and the floodplain were installed (see schematic top view in Figure 1). They  
127 are used to distribute the required discharges in the sub-sections, which enables to quickly  
128 establish a uniform flow relative to in a flume with a single inlet. The flow is then canalised  
129 by a succession of grids and the free surface oscillations are attenuated by a float. The outlet  
130 consists of two independent adjustable tailgates, one for each sub-section. The separated  
131 tailgates enable a better adjustment of the downstream boundary conditions by reducing the  
132 backwater effects and the lateral mass exchange between the sub-sections at the far end of the  
133 flume.

134 In the present paper, we use a Cartesian coordinate system in which  $x$ ,  $y$  and  $z$  are the  
135 longitudinal, lateral and vertical directions, respectively (as presented in Figure 1).  $x = 0$   
136 immediately downstream from the inlet tanks and  $y = 0$  at the lateral bank of the floodplain.  
137  $z$  is taken along a plan following the mean slope of the flume and obtained by the root mean  
138 square method. The origin of the plan is taken in the main channel.

## 139 2.2. *Measurements devices*

### 140 *Water depth and level*

141 The water depths and the water levels were measured using an ultrasonic probe (Baumer  
142 Electric, UNDK 20I 6912 S35A). The uncertainty of the probe was estimated to  $\pm 0.42$  mm  
143 for a recording time greater than 20 s.

### 144 *Mean and instantaneous velocity*

145 A micro-propeller (Nixon, Streamflo Velocity Meter 403) was coupled to a vane and an  
146 encoding angle device for simultaneously measuring the flow direction and the mean  
147 velocities. The recording time was set to between 60 s and 90 s – depending on the lateral  
148 position in the flume – to ensure an accurate estimation of the mean and standard deviation of  
149 the velocity. With such recording time, the uncertainties were estimated to 1.5 % of the mean  
150 velocity.

151 Measurements of instantaneous velocities were performed using a 2D side-looking  
152 Acoustic Doppler Velocimeter (micro-ADV, Nortek, Vectrino+). The sampling frequency  
153 was set to 100 Hz with a signal-to-noise ratio greater than 20 dB in order to have weak  
154 influences of the noise (McLelland and Nicholas 2000). The recording time was set at least to  
155 3 min to ensure an accurate estimation of the mean and standard deviation of the signal.

156 The uncertainties for the estimated Reynolds stresses from the instantaneous  
157 velocities were minimised. The measured velocity signals were despiked using the method of  
158 Goring and Nikora (2002) and the probe misalignment was estimated and corrected using the  
159 methods presented in Peltier (2011).

#### 160 *Boundary shear stress*

161 The boundary shear stress was measured with a Preston tube (outer diameter of 2.72 mm)  
162 using the calibration law specified by Patel (1965). For each experiment, the Preston tube was  
163 aligned with respect to the longitudinal direction and the uncertainty was within 6 % of the  
164 measured boundary shear stress (Preston 1954). In case of large lateral velocities, a correction  
165 coefficient was applied to the pressure measurements for taking into account the fact that the  
166 Preston is no longer aligned with the main flow direction. The correction coefficient was  
167 worked out by measuring the resulting pressure when the Preston tube was turned by a known  
168 angle in a uniform flow.

#### 169 *Measurement grid*

170 The measuring devices were mounted on a movable carriage moving on a metal frame in the  
171 vicinity of the flume. This metal frame is independent of the flume and has the same  
172 longitudinal mean slope as the flume. The carriage was programmable and was moved  
173 through a DC motor with an accuracy of  $\pm 0.2$  mm in both  $x$ - and  $y$ -directions.

174 Along the  $y$ -axis, the grid-step of the measurements was 5 or 10 cm from  $y = 0.05$  m  
175 to  $y = 0.75$  m, 1 cm from  $y = 0.75$  m to  $y = 0.85$  m (the junction between the sub-sections is  
176 at  $y = 0.8$  m) and 2.5 or 5 cm from  $y = 0.85$  m to  $y = 1.15$  m. The grid-step along the  $x$ -axis  
177 was not regular and depends on the measuring device used. The water depth and the mean  
178 velocity were measured at every 0.5 m from  $x = 1.5$  m to  $x = 3.5$  m (the embankment is  
179 placed at  $x_e = 2.5$  m) and then at every 1 m until the end of the flume. The instantaneous  
180 velocity and the boundary shear stress were measured in four cross-sections: one upstream  
181 from the embankment at  $x = 2$  m, one in the embankment cross-section at  $x = x_e = 2.5$  m and  
182 two downstream from the embankment at  $x = 4.5$  m and 6.5 m. Along the  $z$ -axis, the velocity  
183 was measured at least at 2 vertical positions on the floodplain for the shallowest case and at 6  
184 vertical positions for the deepest case.

#### 185 *2.3. Flow conditions*

186 The total discharge and the length of the embankment were chosen in order to examine a  
187 large range of flow conditions, with in particular a large mass exchange between sub-sections.  
188 In these experiments, the mass exchange was generated by a transverse embankment set on

189 the floodplain and the intensity of the lateral mass exchange was inversely proportional to the  
190 longitudinal length of the recirculation zones developing on both sides of the embankment  
191 (upstream:  $L_x^u$  and downstream:  $L_x^d$ ). The recirculation zones were identified by Large Scale  
192 Particle Image Velocimetry (LSPIV); they are bounded by the floodplain wall and the  
193 separation streamline corresponding to zero-discharge in the recirculation zone.

194 The flow conditions are summarized in Table 1. Three reference flows with no  
195 embankment were first investigated. The three values of the total discharge,  $Q_t$ , and discharge  
196 ratio on the floodplain,  $Q_f/Q_t$ , were those to have uniform flows with the relative flow depths  
197  $H_r = 0.2, 0.3$  and  $0.4$ , respectively. The downstream tailgates were adjusted so that the mean  
198 slope of the water surface was equal to the longitudinal bed-slope. Six flows with a thin  
199 obstacle, representing an embankment on the floodplain, were further investigated. The  
200 embankment was set at  $x_e = 2.5$  m, perpendicularly to the longitudinal direction. Various  
201 lengths of embankment,  $d$ , were investigated (see the fourth column in Table 1), with the  
202 boundary conditions used for the reference flows, *i.e.* the same upstream discharge  
203 distributions and height of the tailgates.

204 To analyse the flow conditions, we first consider the longitudinal lengths of the  
205 recirculation zones that develop upstream ( $L_x^u$ ) and downstream ( $L_x^d$ ) from the embankment  
206 (see the fifth and sixth columns in Table 1).  $L_x^u$  is close to  $d$  for the upstream recirculation  
207 zone and the lateral extent  $L_y(x)$  is never larger than  $d$ . By contrast,  $L_x^d$  increases with the total  
208 discharge and the embankment length, and the lateral extent  $L_y(x)$  of the downstream  
209 recirculation zone can reach  $1.1 \times d$  between  $x = 2.75$  m and  $x = 3.25$  m for the six flow-cases  
210 with an embankment (not shown in Table 1). This generates a constricted cross-section in the  
211 flow. Regarding the normalised length  $L_x^d / d$ , it decreases with increasing  $d/B_f$  or decreasing  
212  $Q_t$ , therefore emphasising the role of the bed-generated turbulence in the development of the  
213 recirculation zone (Chu *et al.* 2004, Rivière *et al.* 2004, 2011). Considering the Reynolds  
214 number in the sub-sections,  $R_i = 4R_i U_i / \nu$  ( $\nu$  the kinematic viscosity,  $U_i$  and  $R_i$  respectively the  
215 mean velocity and the hydraulic radius in a subsection), the values in the main channel are  
216 one order of magnitude greater than those on the floodplain (see seventh and eight columns in  
217 Table 1). However, the Reynolds numbers in both sub-sections are sufficiently high to neglect  
218 viscosity effect in the computation of the stresses. Finally the minimal and the maximal  
219 relative flow depths (last column in Table 1) indicate very weak longitudinal variations in the  
220 flow depth for the reference flows, while significant variations are observed for the flow-  
221 cases with an embankment: for such flow conditions, the depth on the floodplain can be twice  
222 higher than that measured without an embankment.

223 In the following sections, the flow-cases are referenced in the form  $Q/d$ , where  $Q$  is  
224 the total discharge and  $d$  the embankment length. Reference cases have  $d = 0.0$  (see in Table  
225 1).

### 226 3. A rapidly varied flow

227 In this section, we show how the embankment set on the floodplain generates a rapidly varied  
228 flow on the floodplain and in a lesser extent in the main channel.

#### 229 3.1. Water depth and level

230 The left plots in Figure 2 show the longitudinal variations in the floodplain water depth,  $H_f$ .  
231 Putting aside the most downstream position and the three first meters for flow-case 17.3/0.0, a  
232 constant flow depth (to the uncertainty) is observed in the flume for the reference flows. The  
233 increase in depth at the end of the flume is due to a slight backwater effect caused by the  
234 difference in level between the bottom of the flume and the bottom of the tailgates. Regarding  
235 the decrease in depth at the inlets (particularly marked for 17.3/0.0), it is due to the grids in  
236 the reservoir that induce a strong head loss and a plunging flow at the channel entrance. For  
237 the embankment-cases, the embankment induces strong variations in the water depth and the  
238 distortions (relative to the reference flows) are felt until the end of the flume. On the  
239 floodplain near the embankment the longitudinal mean slope of the free surface,  $S_{wx}$ , is one  
240 order of magnitude greater than the longitudinal mean slope of the bed ( $S_{ox} = 0.18\%$ ) and the  
241 steepness of this slope increases with both the embankment length ( $S_{wx} \approx 1.5\%$  for 24.7/0.3  
242 and  $S_{wx} \approx 3\%$  for 24.7/0.5) and the total discharge ( $S_{wx} \approx 1\%$  for 17.3/0.3 and  $S_{wx} \approx 4\%$  for  
243 36.2/0.3). It is interesting to see that the water depth at the end of the flume is  
244 equivalent to the uniform one for most flows with an embankment. This seems to  
245 indicate that, in our short flume, the recirculation is hardly affected by any backwater  
246 effects coming from the downstream condition, though a uniform lateral velocity  
247 profile is not recovered.

248 The lateral distribution of the water level,  $Z$ , is shown in four cross-sections in Figure  
249 2 (right plots) for flow-cases 24.7/0.3, 24.7/0.5 and 36.2/0.3. The lateral mean slope of the  
250 free surface,  $S_{wy}$ , can be of the same order of magnitude as  $S_{ox}$  in the zone of large lateral  
251 velocities. This slope increases with both the embankment length ( $S_{wy} \approx 0.25\%$  for 24.7/0.3  
252 and  $S_{wy} \approx 1\%$  for 24.7/0.5) and the total discharge ( $S_{wy} \approx 0.2\%$  for 17.3/0.3 and  $S_{wy} \approx 0.8\%$   
253 for 36.2/0.3). A transverse flow is observed from high water level areas to low water areas,  
254 except at  $x = 4.5$  m for 36.2/0.3, where the presence of a normal undulated hydraulic jump at  
255 this station makes locally rise the water level (see subsection 3.3).

### 256 3.2. Depth-averaged velocity

257 Figure 3 shows the 2D fields of the longitudinal and lateral depth-averaged velocities ( $U_d$ ,  $V_d$ ).  
258 The embankment and the resulting recirculation zones (Table 1) are responsible for large  
259 variations in the flow section, therefore leading to significant lateral depth-averaged velocities  
260  $V_d$ . In the vicinity of the embankment tip,  $V_d$  can be up to 50 % of the longitudinal depth-  
261 averaged velocities  $U_d$ . The flow in the main channel is less influenced by the obstacle and  $V_d$   
262 is rather close to 10 % of  $U_d$ . The sign of  $V_d$  must be referenced relative to the contracted  
263 cross-section located between  $x = 2.75$  m and  $x = 3.25$  m (where  $L_y(x) = 1.04-1.1 \times d$  see in  
264 Figure 3): upstream from the contraction, the lateral velocities are positive and the flow  
265 converges from the floodplain towards the main channel; downstream, the flow diverges from  
266 the main channel towards the floodplain.

267 The comparison of the distribution of the longitudinal depth-averaged velocity with  
268 the reference flow emphasises that as long as a recirculation zone is present in the  
269 measurement cross-section the velocity difference,  $U_m - U_f$ , decreases while the maximum of  
270 the velocity gradient within the mixing layer,  $\partial U_d / \partial y$ , increases. Indeed  $\partial U_d / \partial y$  also  
271 depends on the width of the mixing layer that develops between the channel sub-sections.  
272 This width is also modified by the embankment, as shown in section 4.

### 273 3.3. Froude number

274 A typical distribution of the local Froude number,  $F = \sqrt{U_d^2 + V_d^2} / \sqrt{gh}$  ( $h$  the local water  
275 depth), is presented in Figure 4 (flow-case 24.7/0.3). Because of the large velocities (see in  
276 Figure 3) and the relatively low water depths on the floodplain (see  $H_f$  in Figure 2), Froude  
277 numbers higher than 0.5 are found for all flow-cases with the embankment. Moreover, the  
278 flow becomes supercritical from the contraction until at least the half of the downstream  
279 recirculation zone. This supercritical zone expands with both the total discharge and the  
280 embankment length. The transition from the supercritical to the subcritical regime is operated  
281 through a normal undulated jump consistent with the maximal Froude number smaller than  
282 1.7 (Graf and Altinakar 2000). By contrast, the flow in the main channel is always subcritical.

### 283 3.4. Lateral mass exchange

284 Figure 5(a) shows the longitudinal variation in the floodplain discharge compared to that for  
285 the reference flows,  $100 \times (Q_f - Q_f^{ref}) / Q_f^{ref}$ . The exchange of mass between the sub-sections  
286 occurs until the end of the flume for each case and the longitudinal variation in the floodplain  
287 discharge increases with the embankment length, but decreases with the total discharge. The  
288 minimal floodplain discharge is reached near the contracted cross-section: the floodplain can

289 here lose up to 65 % of its discharge (flow-case 24.7/0.5).

290 To get a deeper insight into the lateral mass exchange, the Figure 5(b) shows the  
291 longitudinal variations in the normalised intensity of the lateral mass exchange per unit  
292 length:

$$293 \quad q_n = -\frac{dQ_f}{Q_f} \quad (1)$$

294 defined at the junction between the sub-sections (a mass exchange from the floodplain  
295 towards the main channel corresponds to  $q_n > 0$ ). In the present experiments, the maximum of  
296  $q_n$  ranges from 0.2 to 0.8, while for non-uniform flows in a straight compound channel, it does  
297 not exceed 0.2 for the most extreme case (Proust *et al.* 2011, 2013): the initial objective of  
298 working with larger mass exchanges is then achieved. The strongest exchanges are observed  
299 in the cross-sections near the embankment and the absolute value of  $q_n$  increases with the  
300 embankment length. By contrast, given the uncertainty on the computation of  $q_n$   
301 ( $\delta q_n = \pm 0.07$ ), it seems that the total discharge has little effect on the variations of  $q_n$ .

### 302 3.5. Time-averaged local velocity

303 The time-averaged longitudinal velocity,  $\bar{u}$ , is displayed in Figure 6 for the flow-case  
304 24.7/0.0 at  $x = 5.5$  m (where the reference flow is almost established; Peltier 2011) and for  
305 the flow-cases 24.7/0.5 at  $x = 2$  m (upstream from the embankment),  $x = 2.5$  m (in the  
306 embankment cross-section) and  $x = 4.5$  m (downstream from the embankment). Notice that  
307 missing data in some of the contour plots in Figure 6, is due to the metrological  
308 considerations: intrusive device and low water depths in some cross-sections. Regarding the  
309 flow-case 24.7/0.0, the inflection of the isovels in the main channel clearly emphasises the  
310 presence of secondary currents of Prandtl's second kind (Tominaga and Nezu 1991). These  
311 secondary current cells are due to the presence of the two vertical solid boundaries in the  
312 main channel. By contrast, the presence of secondary current cells for the flow-cases with an  
313 embankment is not so clear. The lateral mass exchange between the channel sub-sections is  
314 responsible for the weakening of these structures. In the case of the lateral mass exchange  
315 from the floodplain towards the main channel (flow-case 24.7/0.5 at  $x = 2$  m and  $x = 2.5$  m in  
316 Figure 6), some slow water enters the upward part of the main channel until the centreline  
317 (above the bank-full level) and also the downwards part of the main channel near the  
318 floodplain edge, which destroy the secondary currents. The penetration of this slow flow, is  
319 obviously proportional to  $q_n$  (see Figure 5). In the case of the lateral mass exchange coming  
320 from the main channel towards the floodplain (flow-case 24.7/0.5 at  $x = 4.5$  m in Figure 6),  
321 the flow in the main channel and on the floodplain is homogenised by the mass exchange and

322 only boundary layers at the walls can be observed. Once the reattachment point of the  
323 downstream recirculation zone is reached and  $q_n$  is close to zero, the flow in both sub-section  
324 starts establishing a typical compound channel flow.

#### 325 **4. Interaction between a rapidly varied flow and a compound channel flow**

326 In this section, we discuss how the parameters usually studied in compound channel flows are  
327 affected by the lateral mass exchange induced by the embankment on the floodplain.

##### 328 *4.1. Boundary shear stress*

329 Figure 7 first shows typical distributions of boundary shear stress,  $\tau_b$ , measured under  
330 uniform flow conditions with no embankment on the floodplain (at  $x = 4.5$  m). The boundary  
331 shear stress on the floodplain is always smaller than that in the main channel and it increases  
332 with the total discharge. The changes in  $\tau_b$  are smaller in the main channel, since the changes  
333 in the velocity are smaller in the main channel than in the floodplain.

334 Figure 7 then shows  $\tau_b$  for the flow-cases with the embankment 24.7/0.3, 24.7/0.5  
335 and 36.2/0.3. The boundary shear stress on the floodplain at  $x = 2$  m (upstream from the  
336 embankment and  $q_n > 0$ ) decreases compared to those measured for reference flows, because  
337 of the rise in the water depth and of the flow deceleration. This decrease is even larger when  
338 the embankment length is longer or the discharge is higher. By contrast, in the embankment  
339 cross-section, at  $x = 2.5$  m, the boundary shear stress rapidly increases, as the flow here is  
340 plunging and is strongly accelerated close to the bottom. Downstream from the embankment  
341 where  $q_n < 0$ , the boundary shear stresses measured at  $x = 4.5$  m and  $x = 6.5$  m out of the  
342 downstream recirculation zone can be 375 % greater than those measured on the floodplain  
343 under uniform flow conditions. These changes are due to the strong flow acceleration and the  
344 very shallow flow related to the supercritical flow regime (Figure 4). It can be noticed that the  
345 distribution of boundary shear stress on the floodplain does not coincide with the reference-  
346 flow one as long as the downstream recirculation zone has not reattached (see flow-cases  
347 36.2/0.0 and 36.2/0.3 at  $x = 6.5$  m in Figure 7).

##### 348 *4.2. Mixing layer between the sub-sections*

349  $U_1$  and  $U_2$  are the mean longitudinal velocities worked out with the depth-averaged velocities  
350 located in the outside of the mixing layer in the main channel and in the floodplain  
351 respectively. We can define the lateral location  $y_\alpha(x)$  for  $0 < \alpha < 1$  such that the longitudinal  
352 depth-averaged velocity,  $U_d$ , writes:

$$353 \quad U_d(x, y_\alpha(x)) = U_2 + \alpha(U_1 - U_2) \quad (2)$$

354 The width of the mixing layer,  $\delta(x)$ , can be defined as follows (van Prooijen *et al.* 2005):

355 
$$\delta(x) = 2(y_{0.75}(x) - y_{0.25}(x)) \quad (3)$$

356 and the centre of the mixing layer,  $y_c$ , is defined as being equal to  $y_{0.5}$ .

357 The Figure 8(a) shows the longitudinal variations in the mixing layer width,  $\delta(x)$ , for  
358 the embankment-cases, compared to the width,  $\delta^{ref}(x)$ , of the reference flows. As long as the  
359 recirculation zone is present in the measurement cross-section (from  $x \approx x_e - L_x^u$  until  
360  $x \approx x_e + L_x^d$ ),  $\delta(x)$  is smaller than  $\delta^{ref}(x)$ , because the velocity difference,  $U_m - U_f$  (see in  
361 Figure 3), is smaller than that for the reference flows (not shown here); e.g. the flow  
362 contraction induces an increase in the floodplain velocity higher than the increase in the main  
363 channel velocity. Upstream and downstream from this zone,  $\delta(x)$  is either equivalent to  $\delta^{ref}(x)$   
364 or greater, because  $U_m - U_f$  is equal or greater than for the reference flow.

365 The Figure 8(b) then shows that the centre of the mixing layer,  $y_c(x)$ , does not always  
366 follow the geometrical forcing created by the floodplain edge. On the one hand,  $y_c(x)$  is  
367 shifted in the main channel when the normalised intensity of the lateral mass exchange per  
368 unit length  $q_n > 0$  and the shift is proportional to  $q_n$ . On the other hand, it seems to remain on  
369 the floodplain edge for  $q_n < 0$  as observed by Proust *et al.* (2013) in a straight compound  
370 channel with a similar value of  $q_n$ .

371 The shape of the mixing layers that develop in the flow-cases 24.7/0.0, 24.7/0.3 and  
372 24.7/0.5 are displayed in Figure 8(c). The part of the mixing layer on the floodplain is highly  
373 impacted by the lateral mass exchange and for the most extreme cases (see flow-case  
374 24.7/0.5), the mixing layer can even disappear where  $q_n$  is maximum.

### 375 4.3. Reynolds shear stress

376 The Figure 9(a) shows the lateral distribution of the depth-averaged Reynolds shear stress,  
377  $T_{xy}$ , for the three reference-cases at the downstream position  $x = 5.5$  m, where the flows were  
378 established in term of water depth and longitudinal depth-averaged velocity. The lateral extent  
379 of the high shear region between the channel sub-sections is close to  $\delta^{ref}(x)$  (not shown here)  
380 and as observed in the literature for vertical banks, the maximum of  $T_{xy}$  is located at the sub-  
381 sections' junction. The magnitude of the maximum of  $T_{xy}$  is inversely proportional to the  
382 relative flow depth  $H_r$  and is proportional to the velocity difference between the sub-sections  
383  $U_m - U_f$ :  $\max(T_{xy}) = 1.28$  Pa and  $0.57$  Pa,  $U_m - U_f = 0.33$  m s<sup>-1</sup> and  $0.17$  m.s<sup>-1</sup>, and  $H_r = 0.2$   
384 and  $0.4$  for cases 17.3/0.0 and 36.2/0.0 respectively. These results confirm the relationship  
385 between  $T_{xy}$  and  $H_r$  under uniform flow conditions with a constant floodplain width (Shiono  
386 and Knight 1991).

387 The lateral distribution of the depth-averaged Reynolds shear stress,  $T_{xy}$ , is strongly  
388 correlated to the lateral gradient of the depth-averaged longitudinal velocity,  $\partial U_d / \partial y$ . Figure  
389 9(b-d) put into relation  $T_{xy}$  and  $\partial U_d / \partial y$  for the reference flow-cases.  $\partial U_d / \partial y$  is multiplied  
390 by a calibrated constant turbulent eddy viscosity,  $\nu_t$ , equal to  $0.3 \times 10^{-3} \text{ m}^2\text{s}^{-1}$  in order to  
391 respect the dimension of  $T_{xy}$ . The lateral variations in both parameters are similar, therefore  
392 qualitatively confirming the Boussinesq relationship for the reference flows.

393 The lateral profiles of  $T_{xy}$  for the flow-cases 24.7/0.3, 24.7/0.5 and 36.2/0.3 are  
394 displayed in Figure 10 at various locations along the channel. Similarly to the reference flows  
395 (Figure 9(a)), the position of the maximum of  $T_{xy}$  coincides with  $y_c(x)$  (see in Figure 8(b)). By  
396 contrast, the magnitudes of the maximum of  $T_{xy}$  can be 3 or 5 times greater or smaller than  
397 those measured for the reference flows. It can be noticed that a secondary maximum is also  
398 observed on the floodplain downstream from the embankment (see at  $x = 4.5 \text{ m}$  for 24.7/0.5  
399 in Figure 10(c)) and exists as long as the downstream recirculation has not reattached. This  
400 secondary maximum is due to the mixing layer that develops between the recirculation zone  
401 and the main flow.

402 The lateral extent of the high shear region also coincides with the one of  $\delta(x)$ . When  
403  $q_n > 0$  (Figure 10(a)), the lateral extent reduces with an increase in the embankment length or  
404 in the total discharge. By contrast, when  $q_n < 0$ , the variations in the lateral extent are not so  
405 clear (see at  $x = 4.5 \text{ m}$  in Figure 10(c)), because the second mixing layer that develops  
406 between the downstream recirculation zone and the main flow constrains the floodplain flow  
407 and prevents the mixing layer between the sub-sections from spreading too far on the  
408 floodplain.

409 All the modifications undergone by the turbulent exchange within the mixing layer  
410 are due to the changes imposed by the lateral mass exchange to the distribution of the  
411 longitudinal velocity in the flume. The right plots in Figure 10 show the lateral distribution of  
412 the depth-averaged longitudinal velocity,  $U_d$ , in the same cross-sections as those for  $T_{xy}$ . As  
413 shown in Figure 10(a-b: upstream and in the embankment cross-section), the lateral extent of  
414 the high shear region is proportional to the velocity gradient,  $\partial U_d / \partial y$ , and the maximum of  
415  $T_{xy}$  is proportional to  $U_m - U_f$ . When considering the stations downstream from the  
416 embankment (see at  $x = 4.5 \text{ m}$  in Figure 10(c)), the lateral extents of the high shear region can  
417 be smaller than that measured upstream from the embankment although  $\partial U_d / \partial y$  is the same  
418 (flow-case 24.7/0.3). This is due to the presence of the velocity dip in the distribution of  $U_d$   
419 near the sub-sections junction, as demonstrated by Nezu *et al.* (1999). This behaviour is  
420 observed from the contraction to at least the half of the downstream recirculation (*i.e.* while  
421 both mixing layers can interact). Finally, the very large peak of Reynolds stress at the sub-

422 sections' junction at  $x = 4.5$  m for case 24.7/0.5, which is related to an almost discontinuity of  
423 velocity, highlights an extremely high turbulent diffusion that can lead to bank erosion.

## 424 **5. Conclusion**

425 The present paper investigates experiments in a compound open-channel with a transverse  
426 embankment on the floodplain. The embankment creates a rapidly varied flow on the  
427 floodplain, which subsequently interacts with the flow in the main channel. Each varied flow  
428 is compared to the reference flow obtained under uniform flow conditions in the same flume.

429 The embankment and the recirculation zones that develop upstream and downstream  
430 are responsible for a strong lateral mass exchange, which induces significant changes in the  
431 water depth and the velocity distribution across the compound channel, when compared to the  
432 reference flows. The mean slopes of the free surface (lateral and longitudinal) can be one  
433 order greater than the mean bed-slope and the lateral depth-averaged velocity near the  
434 embankment can reach 50 % of the longitudinal depth-averaged velocity. Moreover, because  
435 of the low water depth and the high velocity on the floodplain downstream from the  
436 embankment, a supercritical flow occurs until at least the half length of the downstream  
437 recirculation zone.

438 These changes have also great impacts on the parameters more specific to compound  
439 channel flows. It confirms the implication for flood risk assessment and geomorphology  
440 mentioned in the introduction. While the increase in water depth can reach about 50% in the  
441 floodplain upstream the embankment, the 3D flow at the tip of the embankment and the  
442 acceleration in the supercritical zone downstream, induce boundary shear stresses up to  
443 375 % greater than those of the reference flows. The mixing layer developing at the interface  
444 between the sub-sections is also highly affected by the embankment, the recirculation zones  
445 and the lateral mass exchange. As long as a recirculation zone is present in the measurement  
446 cross-section, the mixing layer width remains smaller than the reference flows one and the  
447 turbulent exchange (*i.e.* depth-averaged Reynolds shear stress) is strongly affected. The  
448 magnitude of the peak of depth-averaged Reynolds shear stress can be up to 5 times greater  
449 than that for the reference flows, while the lateral extent of the high shear region is 100 %  
450 smaller. The peak is besides not always located at the junction: it is shifted in the main  
451 channel when mass is transferred from the floodplain towards the main channel and remains  
452 at the sub-sections' junction in the opposite direction. Nevertheless, the Boussinesq  
453 hypothesis can still be used in first approach for describing the evolution of the high shear  
454 region.

455 Thanks to the present data-set (depth, velocity, boundary shear stress, Reynolds  
456 stress), further work could be devoted to numerically model such rapidly varied compound  
457 channel flows in 1D and 2D-H (Linde *et al.* 2012).

- 458 • Concerning 1D modelling, the description of the turbulent exchange at the interface  
459 between the sub-sections is paramount for calculating the discharge distribution  
460 between sub-sections. The present results are of interest to modellers for improving  
461 its modelling, since for now only the shear at the interface between the sub-sections is  
462 considered (apparent shear stress, mixing length model...), and assumed to be  
463 maximum (Nicollet and Uan 1979, Proust *et al.* 2009).
- 464 • Concerning 2D modelling, we showed that the Boussinesq hypothesis is still valid for  
465 flows with embankment, which is interesting for low-cost modelling in an operational  
466 point of view. We also highlighted the behaviour of the secondary currents in the  
467 presence of an embankment, which could be used to correct the shallow water  
468 equations by adding terms taking into account the dispersion on the vertical of the  
469 horizontal velocities (Peltier 2011).

#### 470 **Acknowledgements**

471 The research was funded by IRSTEA and by the Rhône-Alpes region (SRESR -  
472 EXPLORA'DOC 2008 Bourse Cluster 6). The authors are grateful to F. Thollet and M.  
473 Lagouy for their technical support. The authors also thank the anonymous reviewers for their  
474 advices.

#### 475 **Notation**

476  $b$  = Bank-full height (m)

477  $B$  = Total width of the flume (m)

478  $B_f$  = Width of the floodplain (m)

479  $B_m$  = Width of the main channel (m)

480  $d$  = Length of the embankment (m)

481  $F$  = Froude number (-)

482  $g$  = Gravity constant ( $\text{m}\cdot\text{s}^{-2}$ )

483  $h$  = Local water depth (m)

484  $H_f$  = Water depth on the floodplain (m)

485  $H_m$  = Water depth in the main channel (m)

486  $H_r$  = Relative flow depth (-)

487  $L$  = Longitudinal length of the flume (m)

488  $L_x^d$  = Longitudinal length of the downstream recirculation zone (m)

- 489  $L_x^u$  = Longitudinal length of the upstream recirculation zone (m)  
490  $L_y(x)$  = Lateral extent of the recirculation zones (m)  
491  $q_n$  = Normalised intensity of lateral mass exchange per unit length (-)  
492  $Q_f$  = Discharge on the floodplain ( $\text{m}^3 \cdot \text{s}^{-1}$ )  
493  $Q_t$  = Total discharge ( $\text{m}^3 \cdot \text{s}^{-1}$ )  
494  $R_i$  = hydraulic radius of sub-section  $i$  (m)  
495  $R$  = Reynolds number (-)  
496  $S_{ox}$  = Longitudinal mean bed-slope (-)  
497  $S_{wx}$  = Longitudinal mean free surface slope (-)  
498  $S_{wy}$  = Lateral mean free surface slope (-)  
499  $T_{bi}$  = Mean boundary shear stress in the sub-section  $i$  (Pa)  
500  $-\overline{\rho u'v'}$  = Reynolds shear stress (Pa)  
501  $T_{xy}$  = Depth-averaged Reynolds shear stress (Pa)  
502  $\bar{u}$  = Time-averaged longitudinal velocity ( $\text{m} \cdot \text{s}^{-1}$ )  
503  $u'$  = Fluctuating longitudinal velocity ( $\text{m} \cdot \text{s}^{-1}$ )  
504  $U_d$  = Longitudinal depth-averaged velocity ( $\text{m} \cdot \text{s}^{-1}$ )  
505  $U_f$  = Longitudinal mean velocity on the floodplain ( $\text{m} \cdot \text{s}^{-1}$ )  
506  $U_m$  = Longitudinal mean velocity in the main channel ( $\text{m} \cdot \text{s}^{-1}$ )  
507  $v'$  = Fluctuating lateral velocity ( $\text{m} \cdot \text{s}^{-1}$ )  
508  $V_d$  = Lateral depth-averaged velocity ( $\text{m} \cdot \text{s}^{-1}$ )  
509  $x$  = Longitudinal direction (m)  
510  $x_e$  = Position of the embankment with respect to the inlets (m)  
511  $y$  = Lateral direction (m)  
512  $y_c$  = Centre of the mixing layer between the sub-sections (m)  
513  $z$  = Vertical direction (m)  
514  $\delta(x)$  = Width of the mixing layer between the sub-sections (m)  
515  $\nu$  = Kinematic viscosity ( $\text{m}^2 \cdot \text{s}^{-1}$ )  
516  $\nu_t$  = Turbulent eddy viscosity ( $\text{m} \cdot \text{s}^{-2}$ )  
517  $\rho$  = Fluid density ( $\text{kg} \cdot \text{m}^{-3}$ )  
518  $\tau_b$  = Boundary shear stress (Pa).

## 519 **References**

- 520 Bourdat, A. (2007). Débordements des cours d'eau en présence de remblais routiers dans les  
521 lits majeurs. *Master's thesis*. HHL Y, Cemagref, France.

- 522 Bousmar, D., Wilkin, N., Jacquemart, J. H. and Zech, Y. (2004). Overbank flow in  
523 symmetrically narrowing floodplains. *J. Hydraulic Eng.* 130(4), 305–312.
- 524 Bousmar, D., Rivière, N., Proust, S., Paquier, A., Morel, R. and Zech, Y. (2005). Upstream  
525 discharge distribution in compound channel flumes. *J. Hydraulic Eng.* 131, 408–412.
- 526 Bousmar, D., Proust, S. and Zech, Y. (2006). Experiments on the flow in a enlarging  
527 compound channel. In *River Flow 2006: 3<sup>rd</sup> International Conference on Fluvial  
528 Hydraulics*. 6-8 September, Lisbon, Portugal.
- 529 Chlebek, J., and Knight, D. W. (2008). Observations on flow in channels with skewed  
530 floodplains. In *River Flow 2008: 4<sup>th</sup> International Conference on Fluvial Hydraulics*. 3-  
531 5 September 2008, Cesme-Izmir, Turkey.
- 532 Chu, V. H., Liu, F. and Altai, W. (2004). Friction and confinement effects on a shallow  
533 recirculating flow. *J. Envir. and Eng. Sciences*. 3, 463–475.
- 534 Elliot, S. C. A. and Sellin, R. H. J. (1990). Serc flood channel facility: skewed flow  
535 experiments. *J. Hydraulic Res.* 28(2), 197–214.
- 536 Goring, D. G., and Nikora, V. I. (2002). Despiking acoustic doppler velocimeter data.  
537 *J. Hydraulic Eng.* 128(1), 117–126.
- 538 Graf, W. H., and Altinakar, M. S. (2000). *Hydraulique fluviale: écoulement et phénomènes  
539 de transport dans les canaux à géométrie simple*. PPUR presses polytechniques.
- 540 Hauet, A., Kruger, A., Krajewski, W. F., Bradley, A., Muste, M., Creutin, J. D. and Wilson,  
541 M. (2008). Experimental system for real-time discharge estimation using an image-  
542 based method. *J. Hydrologic Eng.* 13(2), 105–110.
- 543 Knight, D. W., and Demetriou, J. D. (1983). Floodplain and main channel flow interaction.  
544 *J. Hydraulic Eng.* 109(8), 1073–1092.
- 545 Knight, D. W., and Hamed, M. E. (1984). Boundary shear in symmetrical compound  
546 channels. *J. Hydraulic Eng.* 110 (10), 1412–1430.
- 547 Knight, D. W., and Shiono, K. (1990). Turbulence measurements in as shear layer region of a  
548 compound channel. *J. Hydraulic Res.* 28(2), 175–196.
- 549 Lefort, P. and Tanguy, J. M. (2009). Mécanisme de l'écoulement à surface libre. In *De la  
550 goutte de pluie jusqu'à la mer : traité d'hydraulique environnementale. Tome 1 :  
551 processus hydrologiques et fluviaux*. J. M. Tanguy, eds. Lavoisier, Paris, France, 207–  
552 265.
- 553 Linde, F., Paquier, A., Proust, S., and Peltier, Y. (2012). Errors in 2-D modelling using a 0th  
554 order turbulence closure for compound channel flows. In *River Flow 2012: 6<sup>th</sup> Int. Conf.  
555 on Fluvial Hydraulics*. 5-7 September, San José, Costa-Rica. 247-254.
- 556 McLelland, S. J., and Nicholas, A. P. (2000). A new method for evaluating errors in high-  
557 frequency ADV measurements. *Hydrological Processes*. 14, 351–366.

- 558 Nezu, I., Onitsuka, K. and Iketani, K. (1999). Coherent horizontal vortices in compound open  
559 channel flows. In *Hydraulic modeling*. V. P. Singh, I. W. Seo and J. H. Sonu eds. Water  
560 Resources Publications, Colorado, USA, 17–32.
- 561 Nicollet, G., and Uan, M. (1979). Ecoulements permanents à surface libre en lit composés. *La*  
562 *Houille Blanche*. pp. 21–30.
- 563 Patel, V. C. (1965). Calibration of the Preston tube and limitations on its use in pressure  
564 gradients. *J. Fluid Mech.* 23, 185–208.
- 565 Peltier, Y. (2011). Physical modelling of overbank flows with a groyne set on the floodplain,  
566 *Ph. D. thesis*. Université de Lyon, Lyon, France.
- 567 Peltier, Y., Proust, S., Bourdat, A., Thollet, F., Rivière, N. and Paquier, A. (2008). Physical  
568 and numerical modelling of overbank flow with a groyne on the floodplain. In *River*  
569 *Flow 2008: 4<sup>th</sup> Int. Conf. on Fluvial Hydraulics*. 3-5 September 2008, Cesme-Izmir,  
570 Turkey.
- 571 Peltier, Y., Proust, S., Thollet, F., Rivière, N. and Paquier, A. (2009). Measurement of  
572 momentum transfer caused by a groyne in compound channel. In *33<sup>rd</sup> IAHR Congress:*  
573 *Water Engineering for a Sustainable Environment*. 9-14 August 2009, Vancouver,  
574 Canada.
- 575 Preston, J. H. (1954). The determination of turbulent skin frictions by means of pitot tubes. *J.*  
576 *Royal Aero. Society*, 58, 109–121.
- 577 Proust, S. (2005). Ecoulements non-uniformes en lits composés : effets de variations de  
578 largeur du lit majeur. *Ph. D. thesis*. INSA de Lyon, Lyon, France.
- 579 Proust, S., Rivière, N., Bousmar, D., Paquier, A., Zech, Y. and Morel, R. (2006). Flow in  
580 compound channel with abrupt floodplain contraction. *J Hydraulic Eng.* 132(9), 958–  
581 970.
- 582 Proust, S., Bousmar, D., Rivière, N., Paquier, A. and Zech, Y. (2009). Non-uniform flow in  
583 compound channel: a 1D method for assessing water level and discharge distribution,  
584 *Water Resour. Res.* 45(12), 411–424.
- 585 Proust, S., Bousmar, D., Rivière, N., Paquier, A. and Zech, Y. (2010). Energy losses in  
586 compound open channels. *Adv. Water Res.* 33(1), 1–16.
- 587 Proust, S., Peltier, Y., Fernandes, J. N., Leal, J. B., Thollet, F., Lagouy, M. and Rivière, N.  
588 (2011). Effect of different inlet flow conditions on turbulence in a straight compound  
589 open channel. In *34<sup>th</sup> IAHR Congress: Balance and Uncertainty; Water in a Changing*  
590 *World*. 26 June-01 July 2011, Brisbane, Australia.
- 591 Proust, S., Fernandes, J. N., Peltier, Y., Leal, J. B., Rivière, N. and Cardoso, A. H. (2013).  
592 Turbulent non-uniform flows in straight compound open-channels. *Submitted to J.*  
593 *Hydraulic Res.*

- 594 Rivière, N., Proust, S. and Paquier, A. (2004). Recirculating flow behind groynes for  
595 compound channel geometries. In *River Flow 2004: 2<sup>nd</sup> Int. Conf. on Fluvial*  
596 *Hydraulics*. 23-25 June 2004, Napoly, Italy.
- 597 Rivière, N., Gautier, S. and Mignot, E. (2011). Experimental characterization of flow  
598 reattachment downstream open channel expansions. In *34<sup>th</sup> IAHR Congress: Balance*  
599 *and Uncertainty; Water in a Changing World*. 26 June-01 July 2011, Brisbane,  
600 Australia.
- 601 Sellin, R. H. J. (1964). A laboratory investigation into the interaction between the flow in the  
602 channel of a river and that over its flood plain. *La Houille Blanche*. 793–802.
- 603 Shiono, K., and Knight, D. W. (1991). Turbulent open channel flows with variable depth  
604 across the channel. *J Fluid Mech*. 222, 617–646.
- 605 Shiono, K., and Muto, Y. (1998). Complex flow mechanisms in compound meandering  
606 channels with overbank flows. *J. Fluid Mech*. 376, 221–261.
- 607 Tominaga, A., and Nezu, I. (1991). Turbulent structure in compound open channel flow.  
608 *J. Hydraulic Eng*. 117(1), 21–41.
- 609 van Prooijen, B. C., Battjes, J. A., and Uijtewaal, W. S. J. (2005). Momentum exchange in  
610 straight uniform compound channel flow. *J. Hydraulic Eng*. 131(3), 175–183.
- 611

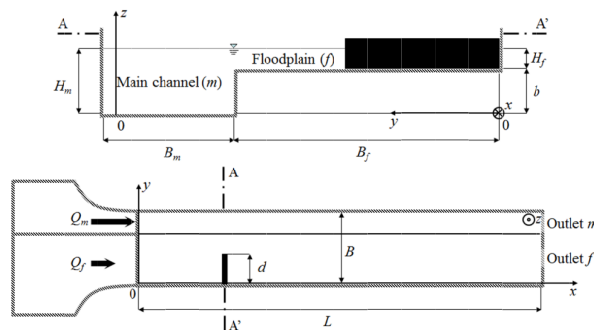
622 Table 1 Main characteristics of the experimental data-set: reference flows (noted  $Q/0.0$ ),  
 623 embankment-cases (noted  $Q/d$ )

	$Q_t$ ( $L \cdot s^{-1}$ )	$Q_f/Q_t$ (%)	$d/B_f$ (-)	$L_x^u/d$ <sup>a</sup> (-)	$L_x^d/d$ (-)	$R_f$ <sup>b</sup> $10^4$ (-)	$R_m$ <sup>b</sup> $10^5$ (-)	$H_r$ <sup>c</sup> (-)
17.3/0.0	17.3	13.9	0	0	0	1.05 - 1.22	1.10 - 1.15	0.21 - 0.23
24.7/0.0	24.7	25.5	0	0	0	2.82 - 3.15	1.32 - 1.40	0.32 - 0.35
36.2/0.0	36.2	38.7	0	0	0	6.36 - 6.75	1.65 - 1.73	0.41 - 0.43
17.3/0.3	17.3	13.9	0.38	1	6	1.06 - 1.73	1.13 - 1.20	0.14 - 0.23
17.3/0.5	17.3	13.9	0.63	1	5	1.16 - 2.34	1.21 - 1.31	0.12 - 0.3
24.7/0.3	24.7	25.5	0.38	1	9.8	2.72 - 3.78	1.26 - 1.42	0.23 - 0.38
24.7/0.5	24.7	25.5	0.63	1	8.3	2.18 - 4.79	1.24 - 1.62	0.21 - 0.45
36.2/0.2	36.2	38.7	0.25	1	15.25	6.18 - 7.47	1.63 - 1.87	0.31 - 0.5
36.2/0.3	36.2	38.7	0.38	1	12.5	5.20 - 7.50	1.69 - 1.92	0.29 - 0.54

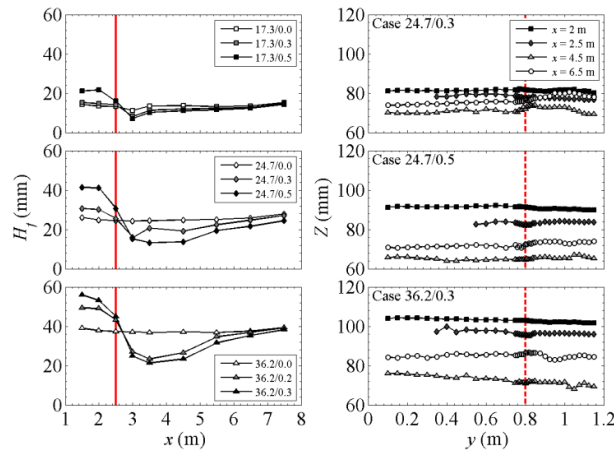
624 <sup>a</sup> The lengths of the recirculation zones were assessed by Large Scale Particle Imaging Velocimetry  
 625 (Hauet *et al.* 2008) using video-sequences of at least 2 min long.

626 <sup>b</sup> Minimum and maximum Reynolds number in the main channel and on the floodplain between  
 627  $x = 1.5$  m and  $x = 7.5$  m.

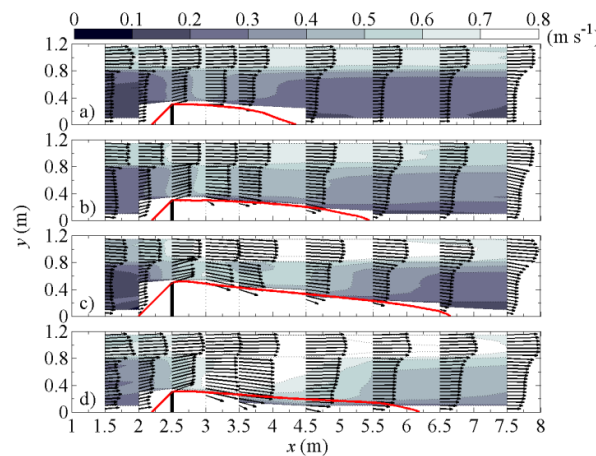
628 <sup>c</sup> Minimum and maximum relative flow depth between  $x = 1.5$  m and  $x = 7.5$  m.



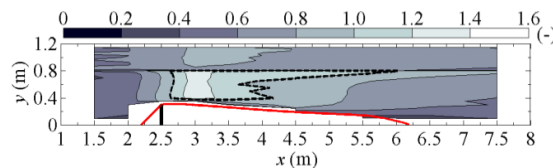
624  
 620 Figure 1 Definition sketch of the flume in the LMFA: cross-sectional and plan views (scheme  
 621 is not to scale).  
 627



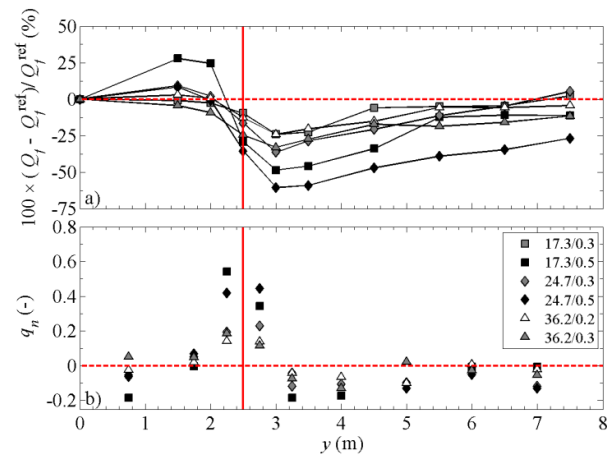
623  
 624 Figure 2 (Left plots) Longitudinal variations in the water depth on the floodplain,  $H_f$ , for the  
 625 nine flow-cases. The black plain line corresponds to the  $x$ -wise position of the embankment.  
 626 (Right plots). Lateral distribution of water level,  $Z$ . The dashed line corresponds to the  
 627 junction of the sub-sections. Uncertainty:  $\delta H = \pm 0.42$  mm and  $\delta Z = \pm 0.42$  mm.



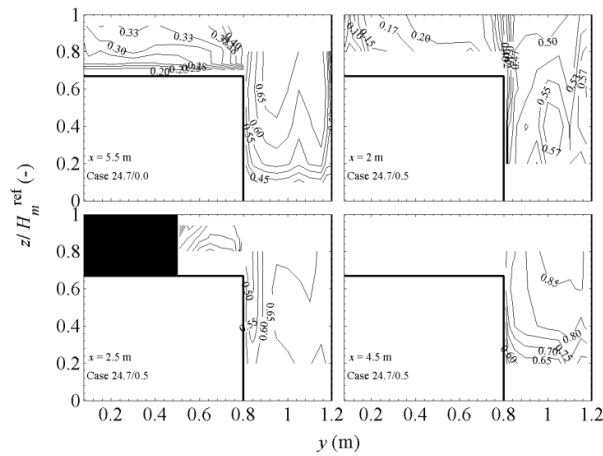
628  
 629 Figure 3 2D depth-averaged velocity fields for flow cases (a) 17.3/0.3, (b) 24.7/0.3, (c)  
 630 24.7/0.5 and (d) 36.2/0.3 (presented in Table 1). The coloured surfaces represent the velocity  
 631 intensity. The separation line between the recirculation zones and the main flow is identified  
 632 by the bold black line. Uncertainty:  $\delta U_d/U_d = \pm 1.5\%$  and  $\delta V_d/V_d = \pm 1.5\%$ .



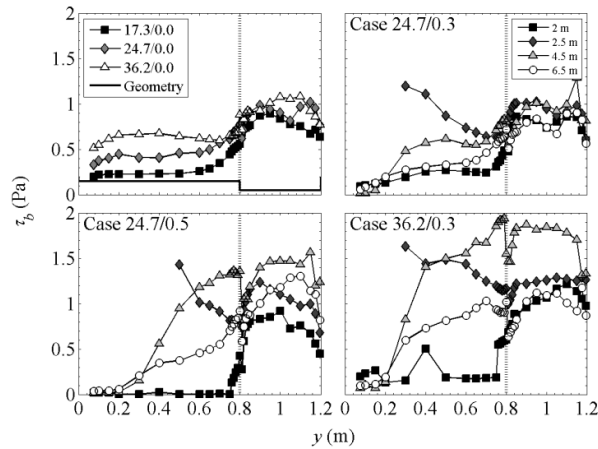
633  
 634 Figure 4 Froude number distribution for flow-case 24.7/0.3 (presented in Table 1). The black  
 635 dashed line corresponds to  $F = 1$ .



636  
 637 Figure 5 (a) Floodplain discharge,  $Q_f$ , compared to that for reference flows,  $Q_f^{\text{ref}}$ . Uncertainty:  
 638  $\delta Q_f / Q_f = \pm 5\%$ . (b) Normalised Intensity of lateral mass exchange per unit length,  $q_n$ , for the  
 639 flow-cases with an embankment. Uncertainty:  $\delta q_n = \pm 0.07$ .

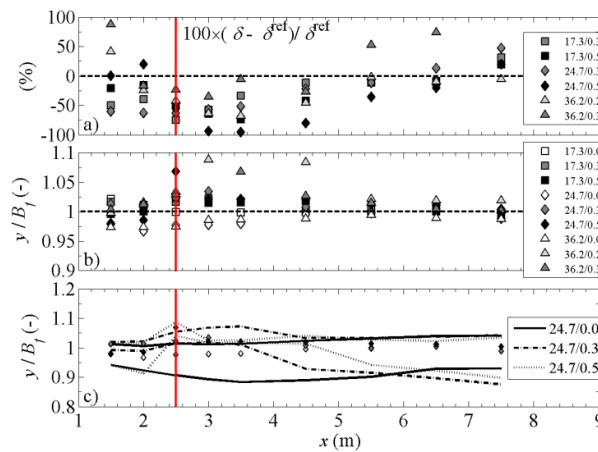


640  
 641 Figure 6 Cross-flow distribution of time-averaged longitudinal velocity,  $\bar{u}$ , for flow-cases  
 642 24.7/0.0 and 24.7/0.5. Uncertainty:  $\delta \bar{u} / \bar{u} = 1.5\%$ .



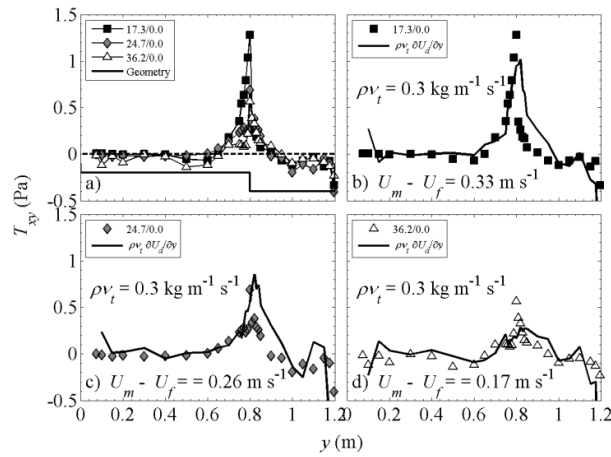
643

644 Figure 7 Lateral distribution of boundary shear stress,  $\tau_b$ , measured under uniform flow  
 645 conditions for flow-cases 17.3/0.0, 24.7/0.0 and 36.2/0.0 and with an embankment for flow-  
 646 cases 24.7/0.3, 24.7/0.5 and 36.2/0.3 (Table 1). Uncertainty:  $\delta\tau_b/\tau_b = \pm 6\%$ .

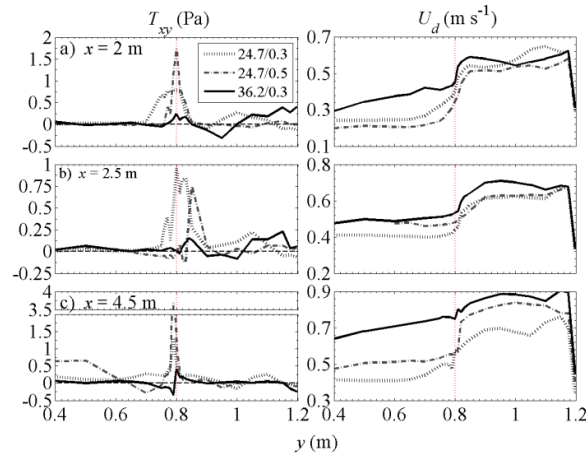


647

648 Figure 8 (a) Longitudinal variations in the width,  $\delta(x)$ , of the mixing layer developing  
 649 between the sub-sections for the flow-cases with an embankment compared to the width,  
 650  $\delta^{ref}(x)$ , of the corresponding reference flows. (b) Position of the centre,  $y_c(x)$ , of the mixing  
 651 layer. (c)  $y_c(x)$  and outer boundaries,  $y_{25}(x)$  and  $y_{75}(x)$ , of the mixing layer for the flow-cases  
 652 24.7/0.0, 24.7/0.3 and 24.7/0.5. Uncertainty:  $\delta\delta(x) = \pm 2.5$  cm,  $\delta y_c(x) = \pm 1$  cm.



653  
 654 Figure 9 (a) Lateral distribution of depth-averaged Reynolds shear stress,  $T_{xy}$ , measured at  
 655  $x = 5.5 \text{ m}$  for the reference flow-cases. (b-d)  $T_{xy}$  compared to  $\partial U_d / \partial y$ .



656  
 657 Figure 10 Lateral distributions of the depth-averaged Reynolds shear stress and depth-  
 658 averaged longitudinal velocities for the flow-cases 24.7/0.3, 24.7/0.5 and 36.2/0.3 at three  
 659 downstream distances.